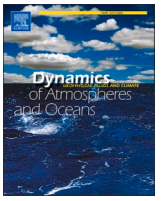
Dynamics of Atmospheres and Oceans 110 (2025) 101561



Contents lists available at ScienceDirect

Dynamics of Atmospheres and Oceans

journal homepage: www.elsevier.com/locate/dynatmoce





New formulas for estimating initial dilution of buoyancy-dominated jets in a current

Galip Seckin [a,*], Cagatayhan Bekir Ersu [a], Irfan Macit [b]

[a] Cukurova University Environmental Engineering Department, Balcali, Saricam, Adana, Turkey
[b] Cukurova University Industrial Engineering Department, Balcali, Saricam, Adana, Turkey

ARTICLE INFO

Keywords:
Modeling
Prediction
Simulation
Outfalls
Dilution

ABSTRACT

For buoyancy-dominated effluents discharged into moving water, three distinct regions are recognized: the buoyancy-dominated near field (BDNF), the buoyancy-dominated far field (BDFF), and an intermediate transition region. Most existing initial dilution formulas—derived from empirical and field studies—focus on the BDNF and BDFF regions while neglecting the transition zone. In this study, two new semi-empirical equations were developed using field and experimental data: one for submerged discharges and another for minimum surface dilution. These equations were calibrated via nonlinear regression, offering a unified approach to effectively calculating initial dilution across both the BDNF and BDFF regions while also addressing the transition region's dilution in a single step. The proposed formulas were further validated through comparison with an earlier semi-empirical model using the same dataset.

1. Introduction

Marine outfall discharges are engineered systems designed to release treated wastewater or industrial effluents into coastal and oceanic environments, often via submerged pipelines extending offshore. These systems rely on buoyant jet dynamics to enhance initial dilution, minimizing environmental impacts by dispersing pollutants into large water bodies (Jirka, 2007; Roberts, 2019). However, despite dilution mechanisms, poorly managed outfalls can lead to localized water quality degradation, affecting marine ecosystems through eutrophication, hypoxia, and bioaccumulation of contaminants (Wu et al., 2021). Regulatory frameworks, such as the Clean Water Act in the U.S. and the European Water Framework Directive, mandate strict effluent standards to mitigate ecological risks (USEPA, 2022; European Commission, 2000). Understanding the interplay between discharge dynamics, ocean currents, and ecological thresholds is critical for sustainable outfall design and environmental protection (Fischer et al., 1979).

When the discharged fluid exhibits a lower density than the surrounding ambient fluid, it generates a buoyant jet. In such cases, the flow dynamics are influenced not only by viscous and turbulent shear forces but also by buoyancy-driven acceleration, which causes the plume to ascend relative to the ambient environment (Jirka, 2004; Lee and Chu, 2003). This buoyancy-induced motion produces a secondary flow structure, wherein the discharged fluid moves relative to the ambient. Consequently, this secondary flow enhances the entrainment of ambient fluid into the jet through both viscous and turbulent shear mechanisms (Fischer et al., 1979).

Two primary entrainment mechanisms—shear entrainment and forced entrainment—govern the initial dilution of buoyant jets in ambient currents. Shear entrainment arises from turbulent eddies generated by velocity shear at the jet-ambient interface and

* Corresponding author.
E-mail address: gseckin@cu.edu.tr (G. Seckin).

https://doi.org/10.1016/j.dynatmoce.2025.101561
Received 18 February 2025; Received in revised form 16 May 2025; Accepted 20 May 2025
Available online 23 May 2025
0377-0265/© 2025 Published by Elsevier B.V.

dominates under stagnant or weak current conditions (e.g., the buoyancy dominated near field, BDNF) (Papanicolaou and List, 1988). In contrast, forced entrainment is driven by the formation of a counter-rotating vortex pair due to jet-current interaction, becoming predominant in stronger currents (e.g., the buoyancy dominated far field, BDFF) (Jirka, 2007). Understanding these mechanisms is essential for estimating initial dilution (typically quantified in terms of centerline or minimum surface dilution) of buoyant jets (Roberts and Toms, 1987).

Fig. 1 illustrates a sectional view of a vertical buoyant jet discharging into a steady, uniform, horizontal cross-current u_a of density ρ_a. Section a-a corresponds to the shear entrainment zone (also referred to as aspirated or Taylor entrainment) and the BDNF region, whereas Section b-b represents the vortex entrainment zone and the BDFF region (Chu and Lee, 1996). A transitional region exists between these two distinct entrainment regimes. The jet's flow characteristics are quantified by the discharge flux (Q), momentum flux (M), and buoyancy flux (B), while u, ρ_0, and c denote the jet velocity, density, and tracer concentration, respectively (Jirka, 2004). The discharge flux (Q) represents the volumetric flow rate of the effluent released from the outfall, typically measured in cubic meters per second (m^3/s) (Jirka, 2007; Fischer et al., 1979). The momentum flux (M) quantifies the inertial force of the discharged fluid per unit density (units: m^4/s^2) (Roberts and Toms, 1987; Lee and Chu, 2003). The buoyancy flux (B) measures the buoyant force driving plume ascent due to density differences between the effluent and ambient water (units: m^4/s^3) (Jirka, 2004; Papanicolaou and List, 1988). The vertical coordinate y defines an arbitrary depth, and H represents the total water column depth above the jet discharge point. l_b is buoyancy dependent length scale characteristic equal to B/u_a^3. Based on length scale analysis, If $y/l_b < <1$, the region is defined as BDNF, whereas for the opposite, $y/l_b > >1$, the region is named as BDFF (Lee and Chu, 2003).

Entrainment mechanisms mentioned above have been often used in the mathematical modeling of buoyant jets in flowing ambient (e.g. Abraham, 1970; Frick, 1984; Lee and Cheung, 1990; Baumgartner et al., 1994). Recently, Huang et al. (1998) used these entrainment mechanisms for estimating initial dilution of a buoyancy dominated jet flow.

Length-scale analysis has gained considerable attention in theoretical studies on initial dilution estimation for round turbulent buoyant jets, particularly in entrainment methods. Fan (1967) pioneered this field with experimental and theoretical work on turbulent buoyant jets in stratified and flowing ambient fluids, laying the groundwork for integral models. Building on this, Lee and Cheung (1990) proposed a generalized Lagrangian model for buoyant jets in currents, capturing complex trajectory and dilution effects. Nash and Jirka (1996) later examined buoyant surface discharges in unsteady flows, demonstrating the significant influence of ambient turbulence on dispersion.

Davis (1999) consolidated fundamental principles for environmental discharge modeling, emphasizing integral and analytical approaches. Further advancements came from Wang and Law (2002), who developed a second-order integral model for round buoyant jets, improving turbulence and entrainment predictions. Meanwhile, computational tools emerged, with Frick et al. (2003) and Lee et al. (2003) introducing Visual Plumes and VisJet/VisFlood, respectively, for 3D visualization of jet/plume behavior using integral modeling. Jirka (2004) contributed CORMIX, an integral model for single round buoyant jets in stratified flows, validated with experimental data—later applied by Roberts and Villegas (2016) in a Buenos Aires outfall case study to optimize effluent dispersion.

Other notable developments include the work of Socolofsky et al. (2008) on double-plume integral model for multiphase plumes and Shao and Law (2014)'s validation of an integral model for horizontal buoyant jets with asymmetric cross-sections. Beyond integral methods, CFD approaches have expanded understanding: Gildeh et al. (2014) used RANS models to simulate turbulent buoyant wall jets, achieving improved near-field mixing accuracy. Yan and Mohammadian (2017) also employed RANS to study confined buoyant jets, finding that lateral walls enhance mixing but limit plume rise. Similarly, Robinson et al. (2015) applied OpenFOAM to marine discharges, demonstrating scalability for real-world outfalls, while Zhang and Adams (1999) successfully modeled near-field plume dynamics using the *k-ε* turbulence model.

Furthermore, Roberts et al. (2010) argued that length-scale models often provide sufficient accuracy for uncomplicated outfall design scenarios and, in some cases, demonstrate greater reliability than computationally more sophisticated modeling approaches. The advantage of this approach is that each length scale can be given a clear physical interpretation (Fisher et al., 1979). This approach allows determining the initial dilution parameters for unstratified moving waters including discharge-momentum-buoyancy fluxes, velocity of jet discharge, ambient current velocity, densities of effluent and ambient water, etc. (e.g., Lee and Cheung, 1991; Lee and Neville-Jones, 1987; Wright, 1977). These initial dilution parameters are defined by length and time. Therefore, the ambient jet

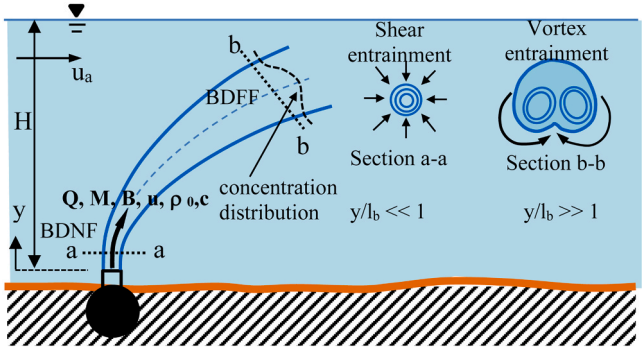


Fig. 1. A sectional view of a vertical buoyant jet discharging into a steady, uniform, horizontal cross-current.

parameters can be physically represented with length scales while representing a specific facet of the overall problem (Wright, 1977; Lee and Cheung, 1991; Mukhtasor et al., 2002).

Lee and Neville-Jones (1987) derived two distinct formulas for the BDNF and BDFF regions through length scale analysis based on field data. Similarly, Lee and Cheung (1991) established separate empirical formulas for the BDNF and BDFF regions using experimental data. In both studies, the transition regions were excluded from the formulation process to maintain analytical clarity. Therefore, the objective of this study was to formulate a single analytical expression that integrates both the BDNF and BDFF regions, replacing the dual formulations proposed by Lee and Cheung (1991) and Lee and Neville-Jones (1987). Furthermore, the transition region is encompassed within a newly derived formula proposed in this study.

1.1. Previous work

Estimation of initial dilution, sometimes called as centerline or minimum dilution (Huang et al., 1998), entails understanding the underlying forces of jets, plumes, and buoyant jets (Roberts et al. 2010). The driving forces for a jet and a plume are source momentum flux and buoyancy flux, respectively, while a buoyant jet is driven by both momentum (M) and buoyancy (B) fluxes (Fischer et al., 1979). Although many methods, for computing initial dilution, were mainly developed based on integral analysis including Lagrange (Lee and Cheung, 1990) and Euler approaches (Davis, 1999), numerical techniques (Fan, 1967; Abraham, 1970; Frick, 1984), length-scale analysis techniques (Roberts, 1979; Roberts et al.,1989a; 1989b; 1989c; Roberts et al. 2010; Wright, 1977; Wright, 1984; Lee and Neville-Jones, 1987) have maintained their popularity because of their simplicity. Furthermore, it is a prominent method that offers applicable answers with little effort despite their ambiguity (Roberts et al., 2010).

In the case of a round turbulent buoyant jet discharged in unstratified moving waters, the initial dilution can be physically represented by the relevant parameters (Lee and Cheung, 1991; Lee and Neville-Jones, 1987; Wright, 1977):

$$S = f(Q, M, B, u, y) \tag{1}$$

The source kinematic fluxes of volume Q, B, and M are defined, respectively as follows:

$$Q = \frac{\pi}{4} d^2 u;\ B = g' Q;\ M = Q * u \tag{2}$$

where d = diameter of port, u = velocity of jet discharge, $g' = g(\rho_a - \rho_0)/\rho_0$ where g is the gravitational acceleration, ρ_a and ρ_0 are densities of the ambient water and effluent, respectively.

If the functional relationship in Eq. (1) is expressed in non-dimensional parameters formed from the various length scales, one possible result is (Wright, 1977; 1984)

$$S = f\left(\frac{l_Q}{l_M}, \frac{l_M}{l_b}, \frac{y}{l_b}\right) \tag{3}$$

where l_Q, l_M, l_b are geometry dependent, momentum dependent and buoyancy dependent length scale characteristics, respectively and given by

$$l_Q = \frac{Q}{M^{1/2}};\ l_M = \frac{M^{3/4}}{B^{1/2}};\ l_b = \frac{B}{{u_a}^3} \tag{4}$$

where u_a is ambient current speed.

To address this complex problem, researchers commonly employ a simplified asymptotic approach. This methodology is particularly advantageous as it reduces the system's dimensionality by strategically eliminating less significant parameters through first-principles physical analysis. By focusing on dominant physical mechanisms and their limiting behaviors, the asymptotic approach yields tractable solutions while preserving the essential dynamics of the system. For instance, if one considers the effects of the jet momentum and the buoyancy separately, the number of independent parameters is reduced. For buoyancy dominated discharges, $l_M/l_b << 1$ and for negligible volume flux, $l_Q/l_b << 1$. The relationship in Eq. (3) then becomes as follows (Lee and Cheung, 1991):

$$S = f(y/l_b) \tag{5}$$

Mukhtasor et al. (2002) indicated that simplification from Eq. (3) to Equation (5) is both physically and statistically acceptable.

Lee and Neville-Jones (1987) pointed out that if y/l_Q is much bigger than 1, then the volume flux is negligible resulting in dominance of M and B in mixing behaviour. Further, if l_M is much smaller than l_b, then y/l_b predominantly governs the mixing behaviour. For $y/l_b << 1$, the buoyancy-induced velocity is larger than the ambient velocity, and flow acts like a pure plume in a stagnant fluid with little advection by the ambient current. This region is defined as buoyancy-dominated near field (BDNF). For $y/l_b >> 1$, the jet moves almost horizontally at a velocity (u_a) while rising under the effect of buoyancy. This region is also defined as buoyancy-dominated far field (BDFF). Such flow regimes are often observed at outfalls in shallow coastal waters or estuaries (Huang et al. 1998).

The current investigation centers on the analysis of experimental and field-derived datasets, as reported in the studies by Lee and Cheung (1991) and Lee and Neville-Jones (1987). These datasets concern buoyancy-dominated jet flows, wherein the contribution of momentum flux is negligible. Consequently, the formulations presented following are exclusively applicable to the BDNF and BDFF

regimes.

Using vertical jets, Lee and Cheung (1991) made a series of experiments covering BDNF, BDFF and transition region between BDNF and BDFF, and collected 107 experimental data. Based on their laboratory experiments, Lee and Cheung (1991) developed two simple formulas for centerline dilution:

$$BDNF_1: \quad \frac{S_c Q}{u_a l_b^2} = 0.10\left(\frac{y}{l_b}\right)^{5/3} for \frac{y}{l_b} < 0.01 \tag{6}$$

or

$$BDNF_2: \frac{S_c Q}{B^{1/3} y^{5/3}} = 0.10 for \frac{y}{l_b} < 0.01 \tag{7}$$

$$BDFF_1: \quad \frac{S_c Q}{u_a l_b^2} = 0.51\left(\frac{y}{l_b}\right)^{2} for \frac{y}{l_b} \gg 1 \tag{8}$$

or

$$BDFF_2: \frac{S_c Q}{B^{1/3} y^{5/3}} = 0.51 \quad \left(\frac{y}{l_b}\right)^{1/3} for \frac{y}{l_b} \gg 1 \tag{9}$$

where S_c = centreline dilution, y = elevation with respect to the discharge port.

Similarly, Lee and Neville-Jones (1987) used H instead of y for 320 field data obtained from horizontal jets and proposed two simple formulas:

$$BDNF: \quad \frac{S_m \quad Q}{u_a l_b^2} = 0.31\left(\frac{H}{l_b}\right)^{5/3} for \frac{H}{l_b} < 5 \tag{10}$$

$$BDFF: \quad \frac{S_m \quad Q}{u_a l_b^2} = 0.32\left(\frac{H}{l_b}\right)^{2} for \frac{H}{l_b} \geq 5 \tag{11}$$

where S_m is minimum dilution in the surface, H is water depth above the discharge.

As can be seen from boundary conditions of H/l_b, either the transition region vanishes or is very short when H is used instead of y. It should be noted that vertical and horizontal jets are practically the same for a buoyancy-dominated discharge (Huang et al. 1998). Therefore, Eqs. 6–11 can be used for both vertical and horizontal jets.

None of the formulas given above does not cover the transition region for $0{,}01 < y/l_b < 1$. Whereas, the transition from near-field to far-field is critical in understanding the spatial extent of buoyant effects and how these flows evolve as they propagate away from the source. Huang et al. (1998) saw this deficiency and developed a formula that also included the transition zone using the Lee and Cheung (1991)'s data. Huang et al. (1998) established a theoretical framework for analyzing submerged, single, round, buoyancy-dominated jets in crossflow by defining a control volume bounded by: (1) the jet discharge port (y = 0), (2) an arbitrary elevation y, and (3) the jet boundary between these sections (Fig. 1). The continuity equation for this control volume was expressed as:

$$SQ = Q + E_s + E_f \tag{12}$$

where S represents the flux-average dilution (source concentration divided maximum local concentration) at elevation y, E_s denotes shear entrainment, and E_f signifies forced entrainment. The authors postulated that ambient currents negligibly influence shear entrainment, allowing the combination $Q + E_s$ to be represented by the stagnant water solution:

$$Q + E_s = \alpha B^{1/3} y^{5/3} \tag{13}$$

where α is an empirical constant.

Through dimensional analysis, forced entrainment was formulated as:

$$E_f = u_a y^2 f(y/l_b) \tag{14}$$

where $f(y/l_b)$ represents the dimensionless forced-entrainment factor. This yielded the non-dimensional continuity equation:

$$\frac{SQ}{u_a y^2} = \alpha\left(\frac{y}{l_b}\right)^{-1/3} + f\left(\frac{y}{l_b}\right) \tag{15}$$

The analysis considered that any characteristic dilution (S_c or S_m) could substitute for flux-average dilution through constant proportionality.

While the functional form of $f(y/l_b)$ remained undefined, its asymptotic behavior was constrained by physical considerations:

As $y/l_b \to 0$, the solution must converge to the stagnant case: $f(y/l_b) \to 0$

As $y/l_b \to \infty$, it must approach the advected thermal solution: $f(y/l_b) \to$ constant

Huang et al. (1998) proposed an empirical formulation satisfying these constraints:

$$f\left(\frac{y}{l_b}\right) \propto \frac{1}{1+a\left(\frac{y}{l_b}\right)^{-b}} \tag{16}$$

where a and b are empirical coefficients. This led to the final predictive equation for centerline dilution:

$$\frac{S_c Q}{u_a y^2} = C_1\left(\frac{y}{l_b}\right)^{-1/3} + C_2\frac{1}{1+a_1\left(\frac{y}{l_b}\right)^{a_2}} \tag{17}$$

Calibration using Lee and Cheung's (1991) experimental data yielded:
$C_1 = 0.10$ (matching Eq. 3), $C_2 = 0.51$ (matching eq. 5),$a_1 = 0.10$, and $a_2 = 2$.
Resulting in the operational form:

$$\frac{S_c Q}{u_a y^2} = 0.10\left(\frac{y}{l_b}\right)^{-1/3} + \frac{0.51}{1+0.10\left(\frac{y}{l_b}\right)^{-2}} \tag{18}$$

Mukhtasor et al. (2002) indicated that although inherent uncertainty because of physical instability (as suggested by field data), the Huang et al. (1998) solution (Eq. 18) provides unique values of dilution in transitional regions. On the other hand, Mukhtasor et al. (2002) stated that Huang et al. (1998) evaluated the goodness of fit of the Eq. (18) subjectively and visually by "trial and error". Unlike Huang et al. (1998)'s modeling approach, Mukhtasor et al. (2002) considered that ambient current must affect the shear entrainment. This implies that the power of the right-hand side of Eq. (18) must be higher than −1/3 so that dilution in a weak current (e.g. BDNF) will be positively correlated, i.e., increasing the magnitude of the current should result in an increase in dilution. Through a series of analytical procedures, very similar to Huang et al. (1998)'s procedure, involving the synthesis of the entrainment hypothesis with dimensional analysis, Mukhtasor et al. (2002) derived a semi-empirical formulation, very similar to Eq. (18), to predict initial dilution as shown in Eq.(19):

$$\frac{S_c Q}{u_a y^2} = 0.13\left(\frac{y}{l_b}\right)^{-0.31} + 0.46\exp\left(\frac{-0.22}{\frac{y}{l_b}}\right) \tag{19}$$

It should be noted that Mukhtasor et al. (2002) did not take 5 important data points in their equation into account with an effort to normalize the residuals by pushing the medians of the average values near 0 using variance reduction technique as can be seen in their paper. Moreover, it was advocated that, upon further analysis of the data, there was inconsistent data in rows 26 through 48 in Table 1 of Lee and Cheung (1991)'s related publication. However, the researchers did not prove the inconsistency of the data and reason well for taking out the outliers. The researchers further suggested that there might be a recording, typing, or calculation error. As a result, their approach is almost identical except for the outliers taken out.

2. Materials and Methods

2.1. Materials

A semi-empirical model was developed in this study to address all three regions for buoyancy derived based on data obtained from the work of Lee and Cheung (1991). The researchers carried out 48 laboratory experiments on a buoyancy-dominated vertical heated water jet in a steady crossflow environment and obtained 107 data points. Their experiments were carried out in a laboratory flume with dimensions of 10 m in length, 0.3 m in width, and 0.45 m in depth. The water depth, however, was held constant at 0.4 m. With this setup, the variation in characteristic jet dilution was studied based on y/l_b. More detailed descriptions of the experiment and the data can be found in Lee and Cheung (1991).

2.2. Methods

In order to develop a new and more acceptable model for the estimation of initial dilution of a buoyancy-dominated jet in moving water, the approaches by Lee and Neville-Jones (1987), Lee and Cheung (1991), and Huang et al. (1998) were initially analysed and compared for their determination ability through using their original datasets and application of Excel software. Moreover, the aspects where these model approaches are superior or inferior to one another have been identified.

Based on the examination of those approaches and the lack of their equations in defining the distribution in transition regions and in all three regions altogether, two alternative semi-empirical formulas were developed using regression. These formulas proposed herein were proven to single-handedly produce statistically better results than those of the others.

Huang et al. (1998) used the parameters ($SQ/u_a l_b^2$ instead of $SQ/B^{1/3}y^{5/3}$ along with y/l_b) of Eq. (3) and (5) when developing Eq. (18). However, Lee and Cheung (1991) used the parameters in Eqs. (4) and (6) in Fig. (4) in their article. Fig. (2) shows the distribution

of data for both cases. To understand which distribution has the better correlation, the correlation formulas in the EXCEL package program were applied to both distributions one by one. As seen in Fig. 2, the highest determination coefficients provided by Huang et al. (1998) (data shown as triangle) and Lee and Cheung (1991) (data as circles) were 0,0105 and 0,8324, respectively. It is obvious that both equations seen in Fig. 2 fail to give strong correlation. On the other hand, this determination gives us the idea that the data represented by black circles is more effective and promising in model development.

3. Results

3.1. First analysis of Lee and Cheung's data

As the term $u_a y^2$ included in Eq. (14) is proportional to $B^{1/3}y^{5/3}$, Eq. (14) can be rewritten as follows:

$$E_f = B^{1/3}y^{5/3}\, f(y/l_b) \tag{20}$$

If Eqs. (13) and (20) are substituted into Eq. (12), the following equation is obtained:

$$SQ = \alpha B^{1/3}y^{5/3} + B^{1/3}y^{5/3}\, f(y/l_b) \tag{21}$$

or

$$\frac{SQ}{B^{1/3}y^{5/3}} = \alpha + f\left(\frac{y}{l_b}\right) \tag{22}$$

Eq. (22), developed in the present study, offers an alternative formulation to Eq. (15) proposed by Huang et al. (1998). While preserving the physical foundations of the original model, this revised expression was derived through rigorous asymptotic analysis supplemented by nonlinear regression techniques, utilizing the experimental dataset of Lee and Cheung (1991). An empirical form for f (y/l_b) in (22) is proposed herein as

$$f\left(\frac{y}{l_b}\right) \propto \beta b^{\left(\frac{y}{l_b}\right)} + c\left(\frac{y}{l_b}\right) \tag{23}$$

Then, Eq. (22) becomes

$$\frac{SQ}{B^{1/3}y^{5/3}} = \alpha + \beta b^{\left(\frac{y}{l_b}\right)} + c\left(\frac{y}{l_b}\right) \tag{24}$$

As evident from Eq. (24), the model coefficients exhibit nonlinear behavior. To ensure a unique and continuous solution, a nonlinear regression technique was employed in this study. Utilizing a least squares optimization framework, this approach provides a systematic and objective methodology, with well-documented solution procedures available in the existing literature. Seckin et al. (2006) also showed that, in some applications (for example, boundary shear stress analysis in open channels), nonlinear regression techniques can give results that are as approximate as formulas developed with the laws of mathematics and physics. In order to obtain model coefficients in Eq. (24), the CurveExpert package program was applied to the data (Lee and Cheung, 1991) represented by black circles. The equation that provided the best result is shown below:

$$\frac{S_c Q}{B^{1/3}y^{5/3}} = 0.53 - 0.43 \left[0.18^{\left(\frac{y}{l_b}\right)}\right] + 0.065 \left(\frac{y}{l_b}\right) \tag{25}$$

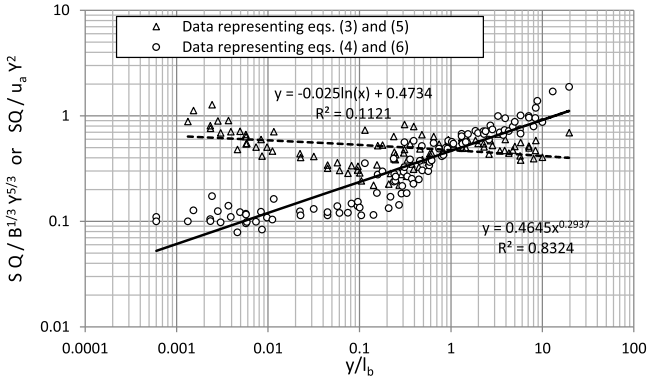


Fig. 2. Formulated outcome of data by Lee and Cheung (1991).

Eq.(18) developed by Huang et al. (1998) and Eq. (25) proposed in this study can be seen together in Fig. 3 for comparison.

The boundary definitions of Eqs. (3–6) for y/l_b show us that the transition region is between 0.01 and 1. The performance of Eq. (25) conforming the data of Lee and Cheung (1991) in this transition region can be better seen in Fig. 4.

Figs. (5) and (6) were created to make a better comparison between Eq. (18) developed by Huang et al. (1998) and the alternative Eq. (25) proposed in this study. Figs. 5 and 6 compare the values found by calculation against the observed data.

3.2. Statistical Analysis

As seen in Fig. 6, there is a very high correlation between the observed data and the data calculated with Eq. (25) (R^2=0.92). However, the coefficient of determination (R^2) between Eq. (18) and the observed data is 0.46. Although Eq. (25) gives a considerably higher correlation coefficient compared to Eq. (18), this result does not mean that Eq. (25) gives better results than Eq. (18). In order to make this decision, it is also necessary to look at the mean absolute error (MAE) and standard error values. When Eq. (25) is statistically compared with Eq. (18), the standard error value for Eq. (25) is 0.099 while it is 0.136 for Eq. (18). MAE is calculated by Eq. (26) below. When Eq. (26) is applied to the observed data, Eq. (18) gives a mean absolute error of 19.93 % and Eq. (25) gives a mean absolute error of 18.43 %.

$$MAE = \left|\frac{Observed\ data - computed\ data}{observed\ data}\right| * 100 \tag{26}$$

The data obtained from the experimental data set were also analyzed using regression residual analysis with machine learning methods in the Jupyter Notebook environment. These data are presented in Fig. 7a. As seen from the Q-Q plot graphical analysis of the residuals of the regression model created from the experimental dataset (data of Lee and Cheung, 1991), the experimental data are scattered along a straight line. The distribution of the data on the straight line indicates that the residuals of the theoretical and experimental data are normally distributed, and the residuals strongly represent the regression model. Additionally, in Fig. 7b, which shows the residual analysis of the data, it can be seen that the points are scattered around zero, indicating that the regression model does not violate the five key rules of the hypothesis (Montgomery, 2009). Thus, it can be inferred that the regression model created from the data set fits the experimental data independently and follows a normal distribution, ~N(0,1). Furthermore, as seen in the regression residual histogram and graphs in Figs. 8a and 8b, there is no auto-correlation among the residual values.

As understood from the residual histogram in Fig. 8a, the residual data approximately follow a right-skewed ~N(0,1) normal distribution. In Fig. 8b, it can be observed that the residual data do not follow any pattern, indicating the absence of autocorrelation. Consequently, the residual analysis of the regression model strongly represents the research.

3.3. Second analysis of Lee and Cheung's data

Assuming that there will be minimum dilution at the surface, Lee and Neville-Jones (1987) used H instead of y in Eq. (3) and (5) for 56 data points for near field and 23 data points for far field, respectively, obtained from horizontal jets and proposed Eqs. (7) and (8) as seen in Fig. (9). As can be seen from boundary conditions of H/l_b, either the transition region vanishes or is very short using H instead of y. This is also seen in Fig. (9).

In the same manner, the approach of Lee and Neville-Jones (1987) was applied to the original 107 experimental data of Lee and Cheung (1991) by using H/l_b instead of y/l_b while H was held constant at 40 cm. Fig. 10 was obtained after regression was carried out.

As seen in Fig. (10), the empirical equation obtained after non-linear regression is;

$$\frac{S_m}{u_a l_b^2}\frac{Q}{} = 382.12\left(\frac{H}{l_b}\right)^{1.9159} \tag{27}$$

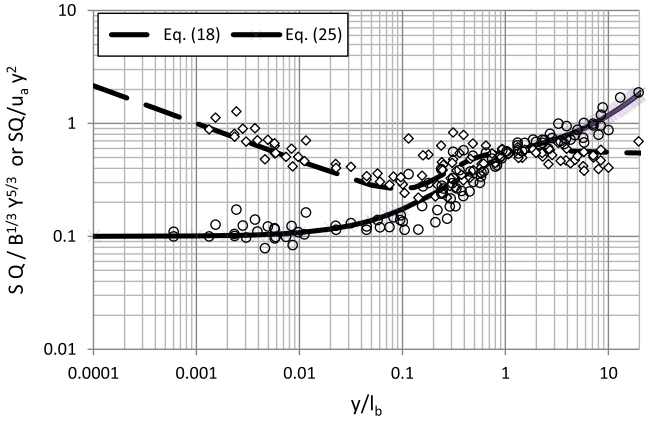


Fig. 3. Presentation of Huang et al. (1998) approach (Eq. 18) and current study (Eq. 25).

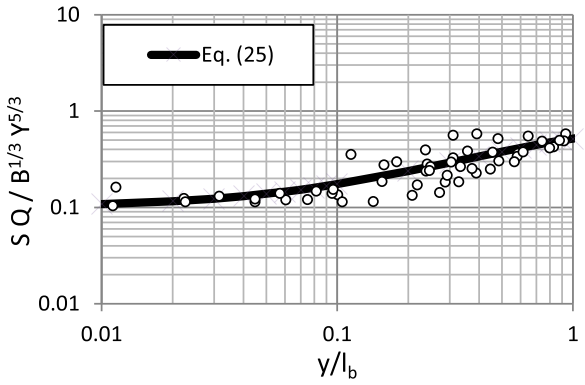


Fig. 4. Performance of Eq. (25) conforming the data of Lee and Cheung (1991) in the transition region.

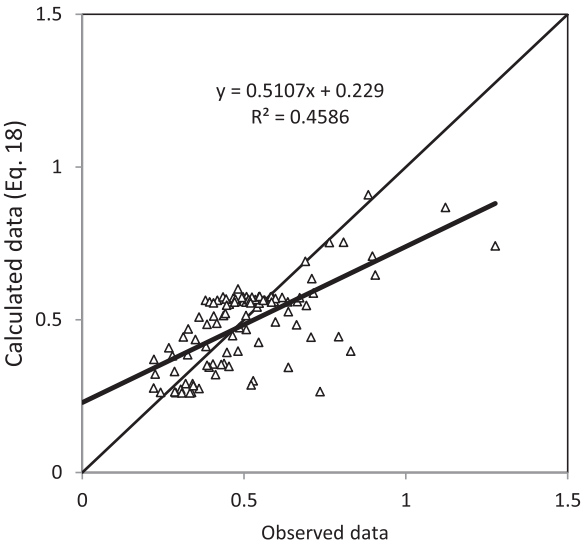


Fig. 5. Comparison of calculated and observed data for the study of Huang et al. (1998).

The application of Eq. (27) to the field data is shown in Fig. 11. Depending on the value of H between 10 cm and 10 m, the line for Eq. (27) will differ and move either upward or downward. In this case, H was held constant at 40 cm per Lee and Cheung (1991) approach.

As seen in Fig. (11), Eq. (27) provides much higher values than the field data. However, it is clear from Fig. (11) that the proposed empirical formula shows an approximately parallel trend with the field data. This suggests that Eq. (27) can be calibrated with the field data using a constant coefficient (ϕ) as follows:

$$\frac{S_m}{u_a}\frac{Q}{l_b^2} = \phi\left[382.12\left(\frac{H}{l_b}\right)^{1.9159}\right] \tag{28}$$

Using the field data, the ϕ coefficient seen in Eq. (28) was determined as 0.0008 by the trial-and-error method. If this value is substituted into Eq. (28), Eq. (29) is obtained:

$$\frac{S_m}{u_a}\frac{Q}{l_b^2} = 0.31\left(\frac{H}{l_b}\right)^{1.916} \tag{29}$$

Then, Eq. (29) was also applied to field data as shown in Fig. 12. As shown in Fig. (12), Eq. (29) shows identical results for field data including BDFF, BDNF, and transition regions. Figs. 9 and 12 clearly indicate that the empirical relationships expressed by Eqs. (7–8) (Lee and Neville-Jones, 1987) and Eq. (29) (current study) both provide a robust fit to the experimental data. Nevertheless, Eq. (29) offers a distinct advantage in that it consolidates the predictive power of two separate equations into a single, more streamlined expression, enhancing both theoretical elegance and practical applicability.

Consequently, the data analyzed in this study were sourced from two previously published investigations. These datasets are

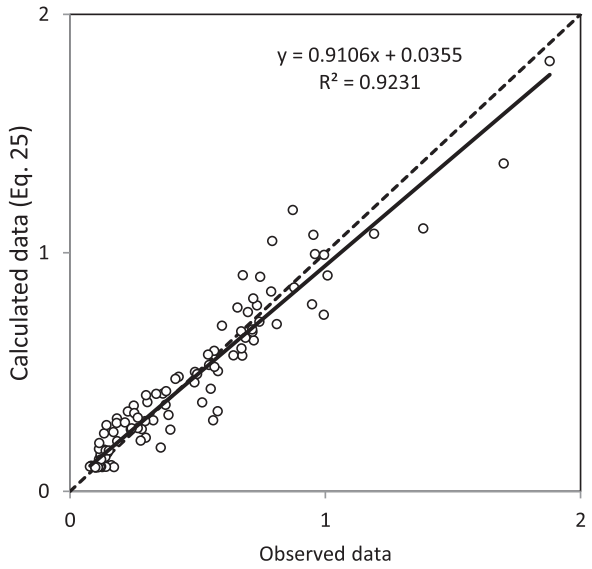


Fig. 6. Comparison of predicted data for current study to observed data of Lee and Cheung (1991).

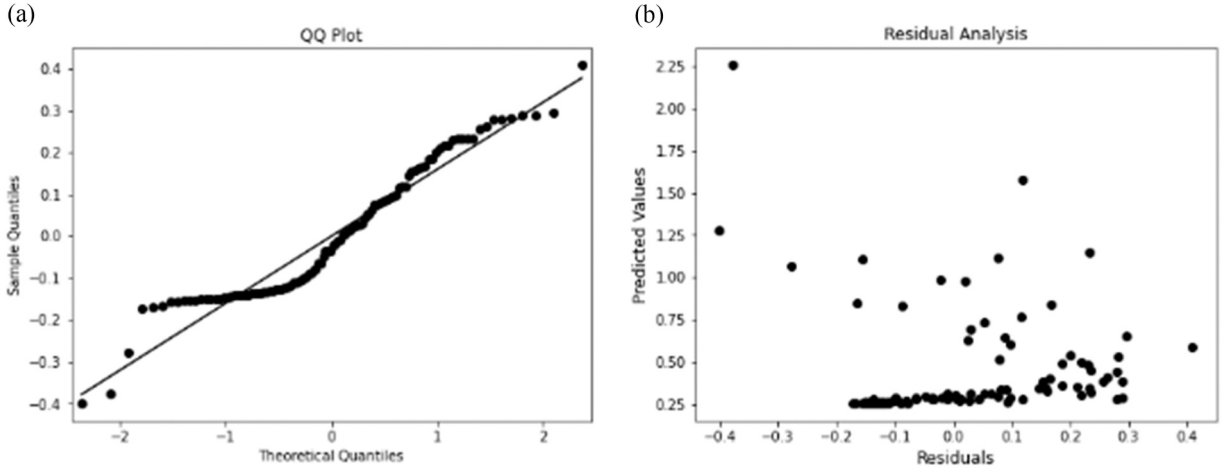


Fig. 7. (a) Q-Q plot analysis; (b) Residual analysis.

particularly notable, as they have been the subject of multiple studies proposing diverse modeling methodologies. The present work was built upon this foundation by identifying opportunities to refine existing modeling approaches and develop a unified framework applicable to all buoyancy-driven jet flows.

4. Conclusion

In the current work, a new semi-empirical formula based on non-linear regression analysis is proposed as an alternative to Eq. (18):

$$\frac{S_c Q}{B^{1/3} y^{5/3}} = 0.53 - 0.43 \left[0.18^{\left(\frac{y}{l_b}\right)}\right] + 0.065 \left(\frac{y}{l_b}\right) \tag{25}$$

This formula can be used for computing initial dilution of buoyancy-dominated jet flow in a current when rising buoyant jet is submerged. This new formula is much better in terms of R^2 (0.92 vs. 0.46) and 1.5 % better regarding mean absolute error. It should be noted that in Lee and Cheung's data, the parameter, l_b, ranges between 0.0006 and 20. However, further research is necessary to extend the analysis to cases where y/l_b exceeds 20, as existing data do not sufficiently cover this regime.

For the minimum surface dilution, the following single formula developed herein can be used as an alternative to Eqs. 7 and 8 eliminating two different borderlines and solutions for near and far-field dilution.

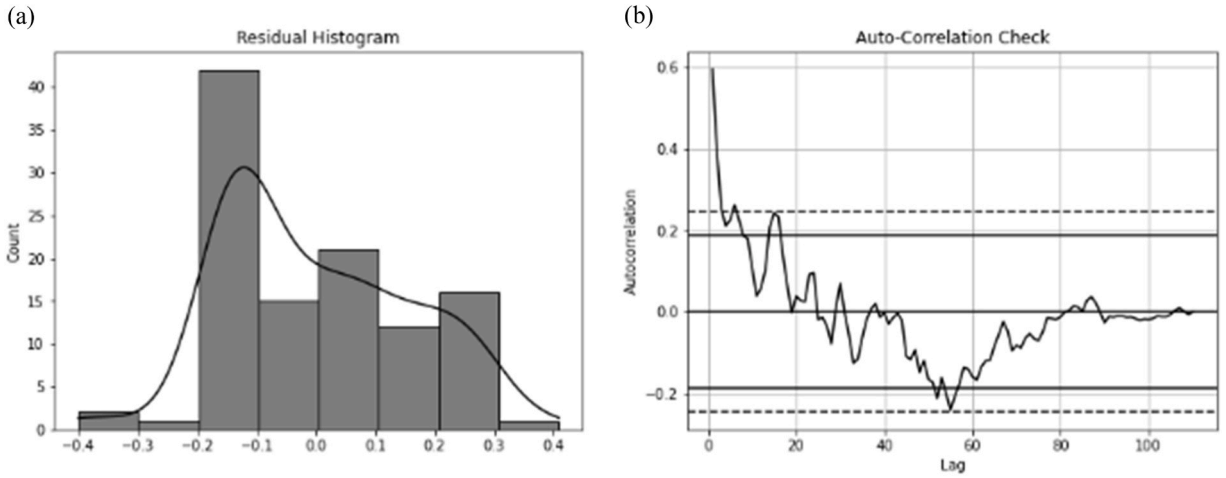


Fig. 8. (a) Residual histogram analysis; (b) Auto-correlation analysis.

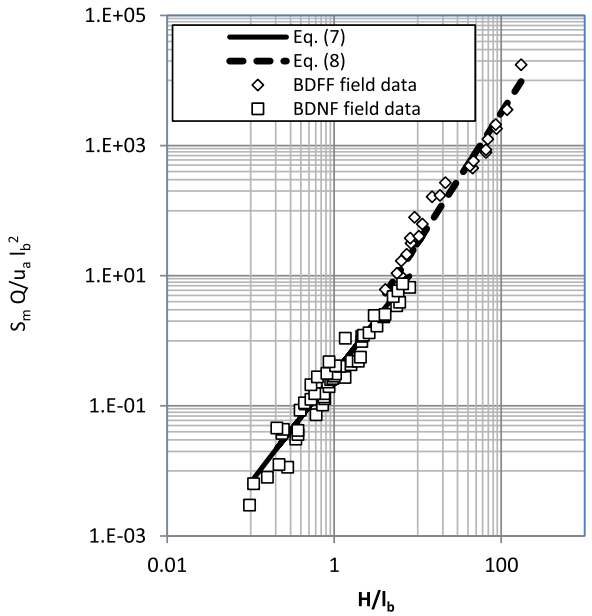


Fig. 9. Graphical presentation of the study of Lee and Neville-Jones (1987).

$$\frac{S_m}{u_a l_b^2} \frac{Q}{} = \quad 0.31\left(\frac{H}{l_b}\right)^{1.916} \tag{29}$$

It is important to note that the proposed formulations in this study are strictly applicable to buoyancy-dominated jet flows. Further investigation is required to develop a unified expression capable of estimating initial dilution across both momentum-dominated near-field (MDNF) and momentum-dominated far-field (MDFF) regions.

CRediT authorship contribution statement

Ersu Cagatayhan: Writing – original draft, Software, Investigation. **Galip Seckin:** Writing – original draft, Supervision, Investigation, Data curation, Conceptualization. **Irfan Macit:** Visualization, Validation, Software, Data curation.

Funding statement

The authors declare no specific funding for this work.

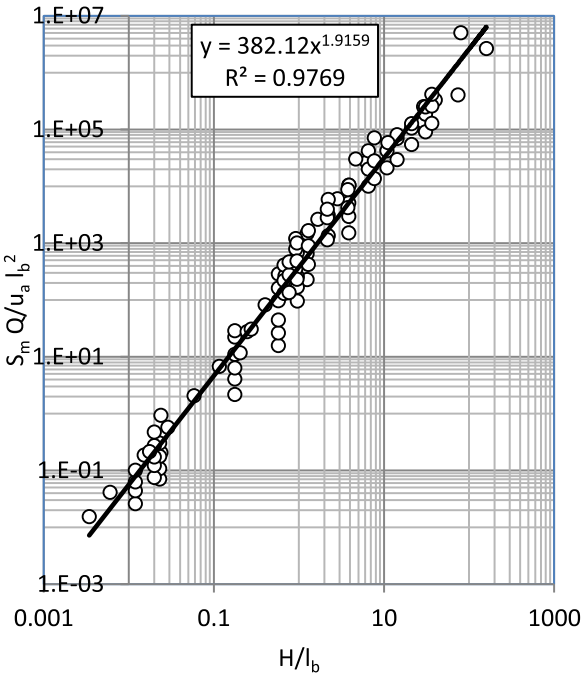


Fig. 10. Graphical presentation of regression analysis to the data of Lee and Cheung (1991) in current study (use of H/l_b instead of y/l_b).

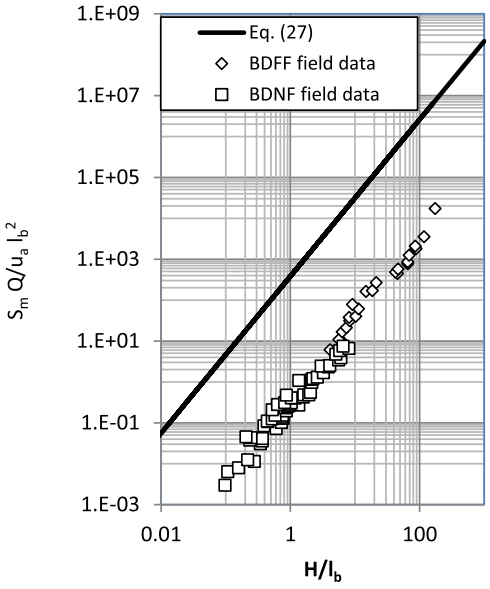


Fig. 11. Application of Eq. (27) found in current study to the field data of Lee and Neville-Jones (1987).

Declaration of Competing Interest

The authors declare that they have no known competing financial interests or personal relationships that could have appeared to influence the work reported in this article.

Data availability

Data will be made available on request.

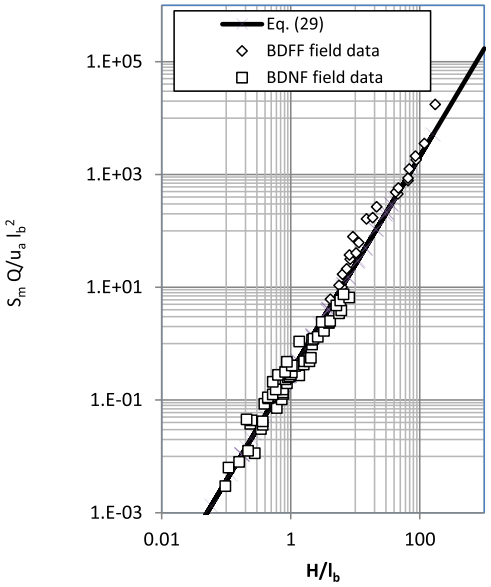


Fig. 12. Application of Eq. (29) found in current study to the field data of Lee and Neville-Jones (1987) after the introduction of calibration coefficient.

References

Abraham, G., 1970. The flow of round buoyant jets issuing vertically into ambient fluid flowing in a horizontal direction. Proc. 5th Int. Water Pollut. Res. Conf. 2, II-1511–III-1517 (San Francisco, Calif.).

Chu, V.H., Lee, J.H.W., 1996. A general integral formulation for turbulent buoyant jets in crossflow. J. Hydraul. Eng. 122 (1), 27–34. https://doi.org/10.1061/(ASCE)0733-9429(1996)122:1(27).

Davis, L.R., 1999. Fundamentals of environmental discharge modeling. Taylor and Francis Group, CRC Press, p. 165. https://doi.org/10.1201/9780203755310.

European Commission, 2000. *Directive 2000/60/EC of the European Parliament and of the Council establishing a framework for Community action in the field of water policy*. In: Official Journal of the European Communities, L327, pp. 1–72.

Fan, L.N. (1967). Turbulent buoyant jets into stratified or flowing ambient fluids. W. M. Keck Laboratory of Hydraulics and Water Resources, California Inst. Tech., Report KH-R-15. ⟨https://doi.org/10.7907/C69V-BE23⟩.

Fisher, H.B., et al., 1979. Mixing in inland and coastal waters. Academic Press, Inc, New York, N.Y.. https://doi.org/10.1016/C2009-0-22051-4

Frick, W., 1984. Non-empirical closure of the plume equations. Atmos. Envir 18 (4), 653–662. https://doi.org/10.1016/0004-6981(84)90252-X.

Gildeh, H.K., Mohammadian, A., Nistor, I., Qiblawey, H., 2014. Numerical Modeling of Turbulent Buoyant Wall Jets in Stationary Ambient Water. J. Hydraul. Eng. 140, 04014012.

Huang, H., Fergen, R.E., Proni, J.R., Tsai, J.J., 1998. Initial dilution equations for buoyancy-dominated jets in current. In: J. Hydr. Engrg, 124. ASCE, pp. 105–108. https://doi.org/10.1061/(ASCE)0733-9429(1998)124:1(105).

Jirka, G.H., 2004. Integral model for turbulent buoyant jets in unbounded stratified flows. Part I: Single round jet. Environ. Fluid Mech. 4 (1), 1–56. https://doi.org/10.1023/A:1025583110842.

Jirka, G.H., 2007. Buoyant surface discharges into water bodies. II: Jet integral model. J. Hydraul. Eng. 133 (9), 1021–1036. https://doi.org/10.1061/(ASCE)0733-9429(2007)133:9(1021).

Lee, J.H.W., Cheung, V., 1990. Generalized Lagrangian model for buoyant jets in current. J. Hydr. Engrg., ASCE 116 (6), 1085–1106. https://doi.org/10.1061/(ASCE)0733-9372(1990)116:6(1085).

Lee, J.H.W., Cheung, V., 1991. Mixing of buoyancy-dominated jets in a weak current. Proc. Instn. Civ. Engrs 91 (2), 113–129. https://doi.org/10.1680/iicep.1991.13585.

Lee, J.H.W., Chu, V.H., 2003. Turbulent jets and plumes: A Lagrangian approach. Kluwer Academic Publishers.

Lee, J.H.W., Neville-Jones, P., 1987. Initial dilution of horizontal jet in crossflow. In: J. Hydr. Engrg, 113. ASCE, pp. 615–629. https://doi.org/10.1061/(ASCE)0733-9429(1987)113:5(615).

Lee, J.H.W., et al. (2003). Visjet and Visflood: Software for Environmental Hydraulic Modeling and Visualization, 7TH ASIAN SYMPOSIUM ON VISUALIZATION, Paper number: conf24a155.

Montgomery, D.C., 2009. Design and Analysis of Experiments, 7th ed. Wiley, New York.

Mukhtasor, M., Lye, L.M., Sharp, J.J., 2002. A new approach to modelling initial dilution of a buoyancy-dominated jet in moving water. J. Environ. Eng. Sci. 1, 101–111. https://doi.org/10.1139/s02-00.

Nash, J.D., Jirka, G.H., 1996. Buoyant surface discharges into unsteady ambient flows. Dyn. Atmospheres Oceans 1996 (24), 75–84.

Papanicolaou, P.N., List, E.J., 1988. Investigations of round vertical turbulent buoyant jets. J. Fluid Mech. 195 (1), 341–391. https://doi.org/10.1017/S0022112088002447.

Roberts, P.J.W., 1979. Line plume and ocean outfall dispersion. Proc. Am. Soc. Civ. Engrs 105 (4), 313–331. https://doi.org/10.1061/JYCEAJ.00051.

Roberts, P.J.W., 2019. Marine outfall systems. In: In Handbook of environmental fluid dynamics, 2. CRC Press, pp. 437–452.

Roberts, P.J.W., Toms, G., 1987. Inclined dense jets in a flowing current. J. Hydraul. Eng. 113 (3), 323–341. https://doi.org/10.1061/(ASCE)0733-9429(1987)113:3(323).

Roberts, P.J.W., Villegas, B., 2016. Modeling and Design of the Buenos Aires Outfalls. J. Hydr. Engrg. ASCE, pp. 05016007–1-17. https://doi.org/10.1061/(ASCE)HY.1943-7900.0001244.

Roberts, P.J.W., Salas, H.J., Reiff, F.M., Libhaber, M., Labbe, A.T., J.C. (2010). Marine Wastewater Outfalls and Treatment Systems. ISBN: 9781843391890. Published by IWA Publishing, London, UK. ⟨https://doi.org/10.2166/9781780401669⟩.

Roberts, P.J.W., Snyder, W.H., Baumgartner, D.J., 1989a. Ocean outfalls. I: Submerged wastefield formation. In: Journal of Hydraulic Engineering, 115. ASCE, pp. 1–25. https://doi.org/10.1061/(ASCE)0733-9429(1989)115:1(1).

Roberts, P.J.W., Snyder, W.H., Baumgartner, D.J., 1989b. Ocean outfalls. II: Spatial evolution of submerged wastefield. In: Journal of Hydraulic Engineering, 115. ASCE, pp. 26–48. https://doi.org/10.1061/(ASCE)0733-9429(1989)115:1(26).
Roberts, P.J.W., Snyder, W.H., Baumgartner, D.J., 1989c. Ocean outfalls. III: Effect of diffuser design on submerged wastefield. In: Journal of Hydraulic Engineering, 115. ASCE, pp. 49–70. https://doi.org/10.1061/(ASCE)0733-9429(1989)115:1(49).
Robinson, D., Wood, M., Piggott, M., Gorman, G., 2015. CFD modelling of marine discharge mixing and dispersion. J. Appl. Water Eng. Res. 4, 152–162, 2015.
Seckin, G., Seckin, N., Yurtal, R., 2006. Boundary shear stress analysis in smooth rectangular channels. Can. J. Civ. Eng. 33, 336–342. https://doi.org/10.1139/l05-110.
Shao, D., Law, A.W.K., 2014. Integral modelling of horizontal buoyant jets with asymmetrical cross sections. Proc. 7th Int. Symp. . Environ. Hydraul., Singap., 7–9. 22.
Socolofsky, S.A., Bhaumik, T., Seol, D.G., 2008. Double-plume integral models for near-field mixing in multiphase plumes. J. Hydraul. Eng. 134 (6), 772–783. https://doi.org/10.1061/(ASCE)0733-9429(2008)134:6(772).
USEPA, 2022 Environmental Protection Agency National Pollutant Discharge Elimination System (NPDES) ⟨https://www.epa.gov/npdes⟩.
Wang, H., Law, A.W.K., 2002. Second-order integral model for a round turbulent buoyant jet. J. Fluid Mech. 459, 397–428.
Wright, S.J., 1977. Mean behavior of buoyant jets in a crossflow. J. Hydr. Engrg., ASCE 103 (5), 499–513. https://doi.org/10.1061/JYCEAJ.0004749.
Wright, S.J., 1984. Buoyant jets in density-stratified crossflow. In: J. Hydr. Engrg, 110. ASCE, pp. 643–656. https://doi.org/10.1061/(ASCE)0733-9429(1984)110:5(643).
Wu, R.S.S., Lau, T.C., Fung, W.K., Ko, P.H., Leung, K.M.Y., 2021. Ecological impacts of marine outfalls: a review. Mar. Pollut. Bull. 167, 112334. https://doi.org/10.1016/j.marpolbul.2021.112334.
Yan, X., Mohammadian, A., 2017. Numerical modeling of vertical buoyant jets subjected to lateral confinement. J. Hydraul. Eng. 143 (7), 04017016 https://doi.org/10.1061/(ASCE)HY.1943-7900.0001307.
Zhang, X., Adams, E.E., 1999. Prediction of Near Field Plume Characteristics Using a k-ε Turbulence Model. J. Hydraul. Res. 37 (1), 21–34.